Chromatographic separation of the platinum-group elements, gold, base metals and sulfur during degassing of a compacting and solidifying igneous crystal pile

Article *in* Contributions to Mineralogy and Petrology · February 1999

DOI: 10.1007/s004100050477

CITATIONS
128

READS
92

2 authors, including:

Alan E. Boudreau
Duke University
113 PUBLICATIONS **3,180** CITATIONS

SEE PROFILE

Contrib Mineral Petrol (1999) 134: 174–185

A.E. Boudreau · W.P. Meurer

Chromatographic separation of the platinum-group elements, gold, base metals and sulfur during degassing of a compacting and solidifying igneous crystal pile

Received: 13 April 1998 / Accepted: 5 October 1998

Abstract The major platinum-group elements (PGE) concentrations in layered intrusions are typically associated with zones in which the sulfide abundance begins to increase. In a number of layered intrusions, there is also a distinct stratigraphic separation in the peak concentrations of the PGE from those of the base metals, gold and sulfur through these zones. These stratigraphic "offsets" are characterized by a lower, typically S-poor, Pt- and Pd-enriched zone overlain by a zone enriched in the base metals, S and Au. The separations amount to a few decimeters to several tens of meters. In some instances, the high Pt and Pd concentrations are associated with trivial amounts of sulfide. Theoretical considerations suggest that these offsets can be modeled as chromatographic peaks that develop during an infiltration/reaction process. Using Pd as a typical PGE and Cu as a typical base metal, a numeric model is developed that illustrates how metal separations can develop in a vapor-refining zone as fluid evolved during solidification of a cumulus pile leaches sulfide and redeposits it higher in the crystal pile. The solidification/degassing ore-element transport is coupled with a compaction model for the crystal pile. Solidification resulting from conductive cooling through the base of the compacting column leads to an increasing volatile concentration in the intercumulus liquid until it reaches fluid saturation. Separation and upward migration of this fluid lead to an upward-migrating zone of increasingly higher bulk water contents as water degassed from underlying cumulates enriches overlying, fluid-undersaturated interstitial liquids. Sulfide is resorbed from the degassing regions and is reprecipitated in these vapor-undersaturated interstitial liquids, producing a zone of relatively high modal sulfide that also migrates upward with time. Owing to its strong preference for sulfide, Pd is not significantly mobile until all sulfide is resorbed. The result is a zone of increasing PGE enrichment that follows the sulfide resorption front as solidification/degassing continues. In detail, the highest Pd concentrations occur stratigraphically below the peak in S and base metals. The high Pd/S ratio mimics values conventionally interpreted as the result of high (silicate liquid)/(sulfide liquid) mass ratios ("R" values). However, in this case, the high Pd/S ratio is the result of a chromatographic/reaction front enrichment and not a magmatic sulfide-saturation event.

A.E. Boudreau (✉) · W.P. Meurer
Division of Earth and Ocean Sciences,
Box 90227, Duke University,
Durham, NC 27708, USA;
Fax: 919-684-5833;
E-mail: boudreau@eos.duke.edu

Editorial responsibility: T.L. Grove

Introduction

The major platinum-group element (PGE; mainly Pd and Pt) concentrations in many layered intrusions broadly occur at levels where sulfide abundance begins to increase. In many instances, the amount of sulfide may be higher than expected cotectic crystallization amounts. The conventional interpretation is that these zones mark levels at which the magma became saturated in an immiscible sulfide liquid (hereafter sulfide) that collected the PGE as it settled to the floor (e.g., Campbell et al. 1983). Alternatively, a number of workers have suggested the PGE may have been carried to the ore zones by volatile fluids (e.g., Ballhaus and Stumpfl 1985, 1986).

In a number of layered intrusions, there is a distinct and characteristic stratigraphic separation of the PGE, base metals, gold and sulfur. Examples of intrusions where this occurs include the Skaergaard intrusion and Kap Edvard Holm complex of East Greenland (Bird et al. 1991, 1995; Andersen et al. 1998), the Great Dyke of Zimbabwe (Prendergast and Wilson 1989) and the Munni Munni complex of Western Australia (Barnes 1993). These stratigraphic separations have been termed "offsets" (Barnes 1993) and are typically characterized by a lower, typically S-poor, Pt- and Pd-enriched zone

overlain by a zone enriched in the base metals, sulfur and gold (Fig. 1). Separations amount to a few tens of centimeters to several tens of meters. The Pt and Pd zones may occur well below the peak in sulfide abundance (which typically corresponds to the peak Cu concentration) and in some instances are associated with trivial amounts of sulfide. Other changes associated with these offsets may include changes in the nature of the sulfide assemblage. For example, the Great Dyke Main Sulfide zone is characterized by a lower troilite-bearing assemblage whereas the overlying assemblages contain pyrrhotite ± pyrite, indicative of a marked increase in sulfur fugacity as a function of height (Oberthür et al. 1998).

Current explanations for the offsets typically invoke small batches of sulfide equilibrating with different parcels of magma with different silicate liquid/sulfide mass ratios (e.g., Prendergast and Keays 1989; Barnes 1993). In these models the PGE are largely incorporated in the first sulfide to precipitate, with sulfide saturation perhaps initiated by a magma mixing event. These models have trouble explaining the observed profiles in detail and have called on a number of questionable assumptions such as requiring "preconcentration" of PGE as alloys in the magma (e.g., Barnes 1993).

In previous works, we suggested that the PGE zones represent a reaction front as volatile fluids exsolved from crystallizing interstitial silicate liquid (hereafter fluid and liquid, respectively), leached sulfur and ore elements, and moved them upward by a process of vapor refining (Boudreau and McCallum 1992; Meurer et al. 1998). In this model, PGE enrichments develop at the front where sulfide-undersaturated fluids removed a preexisting (cumulus) sulfide phase.

Here we expand this model and suggest that PGE - base metal - gold offsets can result from the chromatographic separation of these metals during such a mobilization process. In the following, we first examine the possible chromatographic separation of the PGE and base metals from a theoretical basis using standard infiltration-reaction theory. In the second part of this paper, the results of a numerical model involving the degassing of a solidifying, compacting crystal pile are presented.

Offsets as chromatographic separations

The general features of an infiltration-reaction model have been well described by Godard et al. (1995), a summary of which is presented here. Although Godard et al. were interested in silicate liquid infiltration, the general form of the mass balance equations are indifferent to the nature of the infiltrating medium (fluid or liquid). In the following, the infiltrating phase is considered a fluid.

Consider an upwardly infiltrating fluid that is initially out of equilibrium with the solid + liquid matrix assemblage it is moving through. We define a *reaction zone* as the zone in which reaction between the fluid and host solid + liquid matrix leads to a change in the mineral composition. Where the reaction zone is of minimal

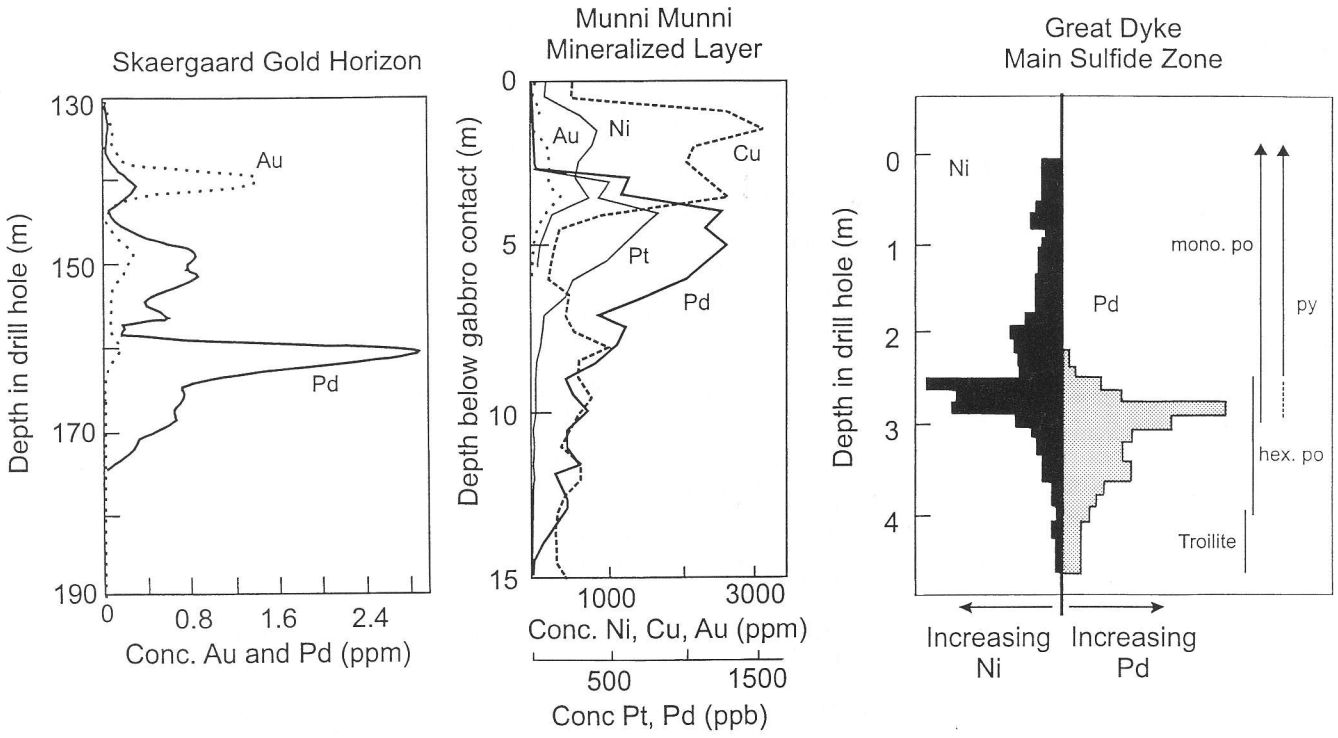

Fig. 1 Examples of PGE, base metal and gold offsets in the Skaergaard intrusion (after Bird et al. 1991), Munni Munni complex (after Barnes 1993) and the Great Dyke (after Prendergast and Wilson 1989; Oberthür et al. 1998)

(infinitesimal) thickness, one may instead speak of a *reaction front*. In the case of interest the reaction zone is defined by the loss of sulfide in the crystal pile; i.e., sulfide is absent below the reaction zone and present above it. Similarly, a *chromatographic* or *chemical zone* or *front* occurs where there is a sharp change in the concentration of a trace element. The mass balance equation for a trace element partitioning between the fluid and the solid + liquid matrix at any point is:

$$\left(\frac{\rho_m}{\rho_f}(1-\Phi)\bar{D}_i+\Phi\right)\frac{\partial C_f^i}{\partial t}+\Phi v_f\frac{\partial C_f^i}{\partial z}-D\frac{\partial\Phi}{\partial z}\frac{\partial C_f^i}{\partial z}$$
$$=\frac{\rho_m}{\rho_f}C_f^i\left((\Phi-1)\frac{\partial\bar{D}_i}{\partial t}+(\bar{D}_i-1)\frac{\partial\Phi}{\partial t}\right) \quad (1)$$

with symbols as defined in Table 1. The first term on the left describes the change in the trace-element concentration in the fluid and matrix and the change in volume of these phases with time. The second and third terms describe the advective and diffusive transport of the element in the fluid, respectively. The right-hand side describes the change in the trace-element concentration because of mineral reactions that change modal variations ($\frac{\partial\bar{D}_i}{\partial t}$) and porosity ($\frac{\partial\Phi}{\partial t}$).

If one neglects diffusion in the fluid phase and assumes that the thickness of the reaction zone is also negligible, then this equation simplifies to

$$\frac{\partial C_f^i}{\partial t}+v_i\frac{\partial C_f^i}{\partial z}=0 \quad (2)$$

where:

$$v_i=\frac{v_f}{1+\theta\bar{D}_i} \qquad \theta=\frac{(1-\Phi)}{\Phi}\frac{\rho_m}{\rho_f} \quad (3)$$

This applies to all regions except at the sharp reaction front, whose position is defined as $z = v_r t$.

To a first approximation, one can consider the regions below and above the reaction front (i.e., the sulfide-absent and sulfide-bearing zones) to each be homogeneous in their properties. In this case, the diffusion coefficient D, v_f and Φ all have constant values in the homogeneous regions on either side of the reaction front. In a plot in the plane (z, t), curves of constant concentration plot as straight lines, the slope of which is the velocity of the chromatographic front for that element in that zone ($\frac{dz}{dt}=v_i$). A given set of trace elements with different bulk partition coefficients, $\bar{D}_i$, will move at different velocities as defined by Eq. 3. High values of the chemical front velocity v_i are associated with small bulk partition coefficients, all other factors being equal (Godard et al. 1995).

Consider the case of the migration of a fluid in a solidifying, partially molten crystal pile, in which fluid is migrating through both a sulfide-free and sulfide-bearing assemblage separated by a dissolution front. We can use metal partitioning between silicate liquid, sulfide and silicate minerals as a good first approximation as to how strongly the metals will be held by the matrix in both regions. From this, one can estimate relative transport rates as the matrix changes. Elements such as Pt and Pd are strongly partitioned into sulfide. Although the partition coefficients are likely a strong function of composition, temperature and oxygen and sulfur fugacity, measured sulfide/silicate liquid partition coefficients in both experimental and natural systems are on the order of $k \sim 10^4$ for Pt and Pd (e.g., Peach et al. 1990, 1994; Fleet et al. 1991). In contrast to Pt and Pd, Cu has a smaller sulfide/silicate liquid partition coefficient

Table 1 List of symbols

C_i	Concentration of element i
D	Diffusion coefficient
$\bar{D}_i$	Bulk distribution coefficient for element i; $\bar{D}_i=\sum_{j=1}^{n}k_d^{ij}X_j$
Q_i	Mass of element i at reaction front
K_f	Permeability of the matrix relative to silicate liquid
K_0	Permeability constant
R	Average grain radius
T	Temperature
c_p	Heat capacity
g	Gravitational acceleration
k_d^{ij}	Phase j/fluid partition coefficient for element i
q	Heat
t	Time
v_f, v_s, v_l	Velocity of fluid, bulk solid and liquid, respectively
v_i, v_i'	Velocity of chromatographic front for element i on each side of reaction front, respectively
v_r	Velocity of the reaction front
z	Height in the cumulus pile
ΔH_{cryst}	Heat of crystallization
ξ^s	Bulk viscosity of the matrix of cumulus crystals
η^s	Shear viscosity of the matrix
f	Liquid fraction
μ	Liquid viscosity
ρ^f, ρ_s, ρ_l, ρ_m	Density of fluid, bulk solid, liquid and solid + liquid matrix, respectively
Φ	Porosity (= fluid fraction)
ψ	Solid fraction
κ	Thermal diffusion coefficient

(k = 180–1383, Rajamani and Naldrett 1978; Peach et al. 1990). The sulfide liquid/silicate liquid partition coefficients for gold are similarly 1–2 orders of magnitude smaller than those for Pd. (e.g., Stone et al. 1990). None of these elements are significantly partitioned into common silicate minerals. Hence, one would expect Pd, Cu and Au to have relatively high chemical velocities in the sulfide-free region compared to the sulfide-poor region. Within the sulfide-bearing region, Cu will have a relatively higher transport velocity than Pd but perhaps be similar to that for Au. This is consistent with the observation that Cu peaks are above PGE peaks but that Cu and Au peaks are broadly coincident. It should be noted however, that relative solubility in the fluid also affects the chemical velocity, as is discussed more fully in the numerical model below.

Consider the case where v_i and v_i' are velocities of element i chromatographic fronts in the sulfide-bearing and sulfide-absent sides of the reaction front, respectively, and v_r is the velocity of the reaction front. In the instance where $v_i < v_r < v_i'$ the enrichment front coincides with the reaction front (Godard et al. 1995). In this special case, where the trace elements are concentrated at the reaction front, the instantaneous concentrations profile is characterized by:

$$\frac{\Delta Q_i}{\Delta t} = C_{f,1}(v_i' - v_r)(\Phi' + (1 - \Phi')\bar{D}_i') + C_{f,0}(v_i - v_r)(\Phi + (1 - \Phi)\bar{D}_i) \quad (4)$$

where $\frac{\Delta Q_i}{\Delta t}$ is the quantity of the trace element accumulated per unit time in the reaction front. The primed quantities denote values for the sulfide-absent zone and unprimed are values for the sulfide-bearing zone. Parameters $C_{f,0}$ and $C_{f,1}$ are the initial concentration of the trace element in the fluid in equilibrium with the original sulfide-bearing assemblage and in the sulfide-undersaturated infiltrating fluid, respectively. Note that the term $(v_i - v_r)$ is negative. Dividing by the velocity of the reaction front gives the increase in the quantity of the trace element as a function of the position of the reaction front:

$$\frac{\Delta Q_i}{\Delta z} = \frac{\Delta Q_i/\Delta t}{v_r} \quad (5)$$

This simply states that the metal content at the reaction front will increase as the reaction front advances with time. Equations (4) and (5) further state that the reaction front contains all the trace element lost from the upstream side of the front. This is essentially the case modeled by Boudreau and McCallum (1992, case #1) for Pd concentrating at a sulfide dissolution front.

In summary, the observed offsets in layered intrusions are consistent with profiles that could develop in an infiltration-reaction environment. Under this interpretation, metal transport is relatively rapid in the sulfide-free regions and the metals are easily carried to the reaction front. Above the front, in the sulfide-bearing region, the distribution of metals largely reflects their transport velocity. The stratigraphic distribution of the offset peaks would suggest that the relative transport velocity of Pt and Pd is less than that of Cu and Au.

A numeric model of element transport during degassing of a compacting and solidifying cumulus pile

The above theoretical description, and especially its simplifications, are strictly true only when the material being infiltrated is uniform on either side of the reaction front and when the infiltrating fluid has an initial constant composition. This situation is not commonly encountered in layered intrusions because fluid evolution is a consequence of crystallization of interstitial liquid. Thus, both the matrix and the exsolved fluid compositions are functions of both time and the location in the crystal pile. Modal changes resulting from crystallization or compaction will result in changes in bulk distribution coefficients independently of any infiltration reactions.

To illustrate more realistically the effects of fluid transport of the PGE and base metals requires a numerical model to evaluate these pertinent variables as a function of time and space. To this end, we have combined the solidification and fluid separation and migration model of Boudreau and McCallum (1992) with the numerical compaction model of Shirley (1986). The following describes the various elements of this model and the results.

Compaction of a cumulus pile

Compaction of a growing cumulus sequence has been modeled by Shirley using the equations derived by McKenzie (1984). The following momentum and continuity equations are used to describe the physical process of compaction:

$$(\xi^s + 4/3\eta^s)\left((1 - f)\frac{\partial^2 v_s}{\partial z^2} - \frac{\partial f}{\partial z}\frac{\partial v_s}{\partial z}\right) = -\frac{\mu f}{K_f}(v_l - v_s) + (1 - f)(\rho_s - \rho_l)g \quad (6)$$

$$\frac{\partial f}{\partial t} = \frac{\partial}{\partial z}[(1 - f)v_s] \quad (7)$$

The left side of Eq. 6 describes how the crystal matrix responds to stress. The terms on the right-hand side describe the buoying effect of the liquid on the matrix as it is driven upward by compaction and the force on the matrix due to gravity. Equation 7 is a continuity equation and is derived from the fact that, in the absence of melting or crystallization, any liquid flux must be compensated for by a matrix flux in the opposite direction so that no voids exist.

The shear and bulk viscosities of the matrix (ω^s and η^s, respectively on the left-hand side of Eq. 6) do not vary greatly within a crystal pile for liquid fractions less than 0.8 (McKenzie 1984). Variations in the permeability (K_f) can result from variations in the rate of accumulation, changes in the initial porosity (e.g., caused

by changes in the mechanism of accumulation), or from variable rates of solidification of interstitial liquid (see below). It is assumed to have a simple functional relationship to liquid fraction:

$$K_f = K_0 \frac{f^3}{(1-f)^2} \tag{8}$$

The density contrast term ($\rho_s - \rho_l$) on the right-hand side of Eq. 6 is taken to be constant throughout the compacting pile in the following calculations. The influence of density changes in the crystal pile have been considered elsewhere (Meurer and Boudreau 1996).

Shirley considered two endmember models, one with a high accumulation rate of crystals relative to the characteristic compaction velocity and one with a low accumulation rate. We have used the parameters for Shirley's "slow accumulation case" (his case 2, with values derived from the Muskox intrusion) in the following numerical modeling (Table 2). They are appropriate for the growth of a large, relatively deep seated and slow cooling layered intrusion. As Shirley has done, we assume that the top of the crystal pile initially starts with a porosity of 60%. During the compaction steps, we ignore the presence and any effects of the fluid phase. Our interest in compaction is largely to model the amount of interstitial liquid available for degassing as a function of depth in the crystal pile.

Heat transport

In the model, the compacting crystal pile is assumed to be cooling through the base. The evolution of temperature with time is governed by two parameters: (1) thermal diffusion; (2) thermal changes involving the latent heat of crystallization. A simplifying assumption is made that the heat capacities of the liquid and solid phases are equal. The small heat capacity contribution of the fluid phase is also ignored because, as described below, it is fractionally removed as soon as it is exsolved. With these simplifications, the evolution of temperature can be expressed by a numerical analog to the following one-dimensional heat transport-reaction equation:

$$\frac{\partial T}{\partial t} = \kappa \frac{\partial^2 T}{\partial x^2} + \frac{\Delta H_{\text{cryst}}}{\rho c_p} \frac{\partial \Psi}{\partial t} \tag{9}$$

where $\frac{\partial \Psi}{\partial t}$ is the rate of change of the mass of crystalline material per unit volume with time. Values for the constants are again as listed in Table 2.

Heat loss from the crystal + liquid assemblage causes crystallization. The change in the amount of crystalline material can be expressed as a function of the gain or loss of heat, q, with time:

$$\frac{\partial \Psi}{\partial t} = \frac{\partial \Psi}{\partial q} \frac{\partial q}{\partial t} \tag{10}$$

where $\frac{d\Psi}{dq}$ is the fraction crystallized per unit heat loss, and $\frac{\partial q}{\partial t}$ is the heat transfer resulting from thermal diffusion. In the following examples, it is assumed that crystallization is a simple function of heat loss such that

$$\frac{\partial \Psi}{\partial q} = \frac{1}{\Delta H_{\text{cryst}}} \tag{11}$$

Volume changes associated with crystallization are ignored. Using nondimensional formulations of Eq. (6) and (7) derived by Shirley (1986), the characteristic time, distance and velocity are given by

$$\bar{t} = \frac{\left(\frac{\xi^s}{K_0}\right)^{1/2}}{R_g(\rho_s - \rho_l)} \tag{12}$$

$$\bar{z} = \left(\frac{K_f \xi^s}{\mu}\right)^{1/2} R \tag{13}$$

$$\bar{v} = \frac{\bar{z}}{\bar{t}} \tag{14}$$

The thermal diffusion coefficient can be scaled to the characteristic compaction length and time scales by:

$$\kappa' = \kappa \frac{\bar{t}}{\bar{z}^2} \tag{15}$$

The effect of heat loss out of the bottom on the evolution of the porosity profile in the cumulus pile is illustrated in Fig. 2. Figure 2a shows the liquid fraction in the crystal pile as well as the dimensionless solid (matrix) and liquid velocity profiles for the case in which there is no heat loss at 20 and 40 dimensionless time steps. The resulting profiles are the same as those of Shirley for his slow accumulation case (accumulation at the top of the crystal pile is at a rate of 0.5 dimensionless velocity units). Figure 2b shows that the consequences of conductive cooling through the bottom are a solidification front that moves upward through the crystal pile. In this and the following model runs, we allow the temperature at the bottom to cool from an initial liquidus temperature of 1250 °C. For the case shown in Fig. 2b, the cooling rate is 5 °C per dimensionless time step. In cases discussed below we vary the cooling/solidification rate relative to the compaction rate to mimic crystallization near or far from a cold bottom contact.

Fluid evolution and element transport

The evolution of fluid from the solidifying interstitial liquid used in the model is as proposed by Boudreau and McCallum (1992). Except as noted below, the initial silicate liquid is assumed to contain 1 wt% water; this is taken as the low end for water contents in boninitic liquids (Sobolev and Chaussidon 1996) and likely to be a realistic water content for many high-Mg layered intrusion magmas (Boudreau et al. 1997). The silicate liquid is assumed to be fluid saturated when its water concentration reaches 5 wt%. Any fluid exsolved immediately migrates upward until it encounters liquid that is not yet fluid saturated. In the model calculations, the mass of fluid that is evolved in one level is assumed to reequilibrate with each overlying zone until it encounters fluid-undersaturated interstitial liquids. On encountering fluid-undersaturated liquid, the sulfur, metal and water content of the fluid is added to the liquid in that zone.

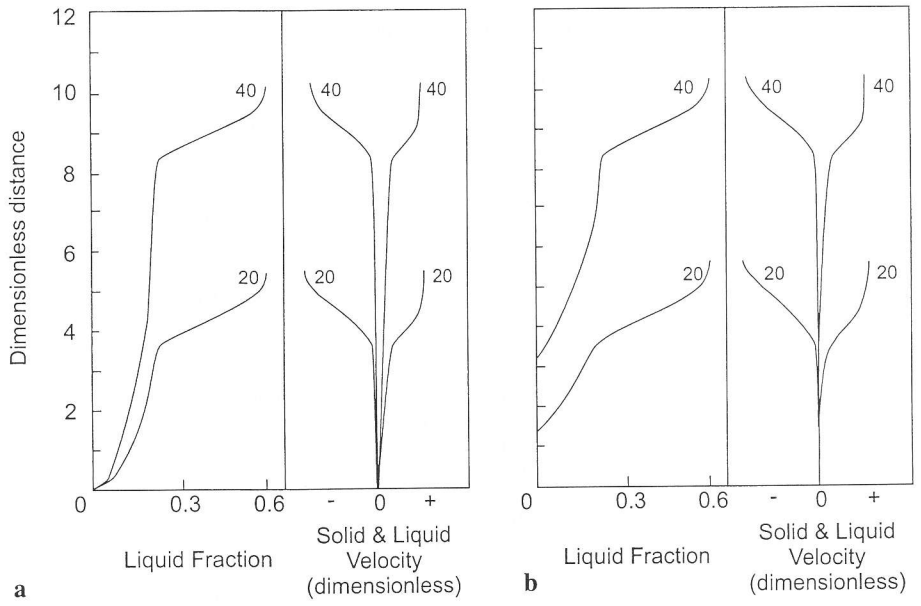

Fig. 2a, b Effect of cooling through the bottom on the distribution of interstitial liquid in a compacting and growing crystal pile. **a** Compaction with no cooling (reproduces case 2 of Shirley, 1986). *Left* plot shows the volume fraction of liquid, *right* plot shows the velocities of the solid (negative velocities) and liquid (positive velocities). Profiles are shown at dimensionless times of 20 and 40. **b** Same parameters as for **a**, but with cooling through the bottom resulting in crystallization of interstitial liquid at the base of the crystal pile. In this case, after 40 dimensionless time steps, the lowermost 3.2 dimensionless units of cumulates have solidified completely

Background bulk sulfur contents of cumulates conventionally interpreted to be sulfide saturated at the time of their formation (and above and away from obviously sulfide enriched zones of interest here) are on the order of a few hundred ppm (e.g., Hoatson and Keays 1989). If these values represent cotectic proportions of sulfide separating from the magma, they imply that sulfur concentrations in the magma were of a similar order. This follows because the magma precipitates sulfide to keep an approximately constant S concentration. In other words, the bulk precipitated assemblage and the magma will both have the same bulk S concentrations. Here we assume sulfide saturation in the silicate liquid occurs at 400 ppm.

The partitioning of metals and S during fractional separation of fluid is modeled over small solidification steps and is treated analogous to fractional melting. The S content is assumed to be 20% by weight of the fluid as long as sulfide is present (based on fayalite-magnetite-quartz-pyrrhotite-O-H-S fluid equilibria calculated by Shi, 1992), otherwise S is assumed to have fluid/liquid partition coefficient of 500. This later partition coefficient is based on the estimated solubility of S in the fluid (20 wt%) to that of sulfide-saturated liquid (400 ppm).

Sulfide/liquid partition coefficients for Cu and Pd are generally as described earlier and are presented in Table 2. For the PGE such as Pt and Pd, metal solubility in silicate liquids is on the order of a few tens to at most a few hundred ppb at oxygen fugacities appropriate for natural magmas (e.g., Borisov et al. 1994; Borisov and Palme 1997). In contrast their solubility in Cl-bearing fluids is highly variable but estimated to be on the order of a few ppm to a few tens of ppm (e.g., Sassani and Shock 1990; Hsu et al. 1991; Ballhaus et al. 1994). This suggests a fluid/liquid distribution coefficient for Pd on the order of 100 is reasonable. However, it should be realized that Pd solubility at these temperatures is not well known. Cu is not likely to be a trace component of any sulfide phase, although it is treated here as such. A value of 80 is used for Cu partition coefficient between fluid and liquid; this value is used so that Cu-S sulfide phase dissolves approximately congruently.

The behavior of an element with a strong sulfide/liquid distribution coefficient such as Pd as compared with that of a base metal such as Cu during degassing is discussed by Boudreau and McCallum and is illustrated in Fig. 3. Shown is the change in the bulk concentration of Pd, Cu and S during solidification and degassing of an interstitial liquid. For this figure alone, the starting assemblage originally contains 25 wt% liquid, 0.1 wt% sulfide (containing 40 wt% S) and the rest solid silicate crystals (no compaction in this case). As discussed by Boudreau and McCallum, fractional separation of a fluid from the interstitial liquid leads to loss of sulfur that in turn leads to resorption of any preexisting sulfide. As the sulfide is the preferred host for Pd, very little Pd is lost to the fluid until most of the original sulfide is lost to the separating fluid. In contrast, Cu is lost approximately in proportion to sulfur loss.

Model results

We now examine four numerical experiments that illustrate some of the features of metal and sulfur transport that can occur during solidification and degassing of a compacting crystal pile.

Case 1, degassing of a sulfide-saturated interstitial liquid in a compacting and solidifying crystal pile

The evolution of water and ore-element concentrations in the crystal pile during solidification is illustrated in Fig. 4. It is assumed that crystallization at the top of the

Table 2 Constants used in numerical models

Compaction parameters (after Shirley, 1986):		
K_0	0.0015	Permeability constant
R	0.0003 m	Average grain radius
g	9.8 m/s^2	Gravitational acceleration
$\xi^s + 4/3\eta^s$	5×10^{15} pa s	Combined bulk and shear viscosity of the matrix
μ	10 pa s	Liquid viscosity
$(\rho_s - \rho_l)$	300 kg/m^3	Density difference between bulk matrix and liquid
Thermal constants:		
κ	1.0×10^{-6} m^2/s	Thermal diffusion coefficient
T	1250 °C	Initial temperature
c_p	100 J/kg	Heat capacity
ΔH_{cryst}	4×10^5 J/kg	Heat of crystallization
Partition coefficients:		
(None are assumed to partition into silicate minerals)		
Pd:		
Sulfide/liquid	10 000	
Fluid/liquid	100	
Sulfide/fluid	100	
Cu		
Sulfide/liquid	250	
Fluid/liquid	80	
Sulfide/fluid	3.12	
S		
Sulfide/liquid	(liquid concentration fixed at 400 ppm while sulfide is present)	
Sulfide/fluid	(fluid concentration fixed at 20 wt% while sulfide is present)	
Fluid/liquid	500 (when sulfide is absent)	

pile produces an assemblage that is sulfide saturated, precipitating 0.1 wt% sulfide (composed of 40% sulfur), and 40% silicate minerals. Compaction reduces the amount of interstitial liquid but crystallization increases the amount of sulfur precipitated as sulfide until fluid saturation is reached.

The solidification of the lower part of the crystal pile leads to an increase in the water content of the intercumulus liquid until it becomes fluid saturated. The fluid migrates upward until it encounters a zone of fluid-undersaturated liquid, at which point it dissolves into that liquid. Also, the increase in the water content of interstitial liquid above the saturated zones causes it to reach fluid saturation earlier in its crystallization. The net effect of this fluid evolution and migration is that a relatively sizable zone of fluid-saturated interstitial liquid develops above the solidified zone and is here termed the "fluid-saturated zone". Note that although the liquid is fluid saturated throughout this zone, the bulk water content of the zone decreases with depth in the crystal pile. This is because: (1) the interstitial liquids are losing volatiles as they solidify and degas; (2) compaction is always working to reduce the amount of interstitial liquid, the only host for water other than the fluid phase.

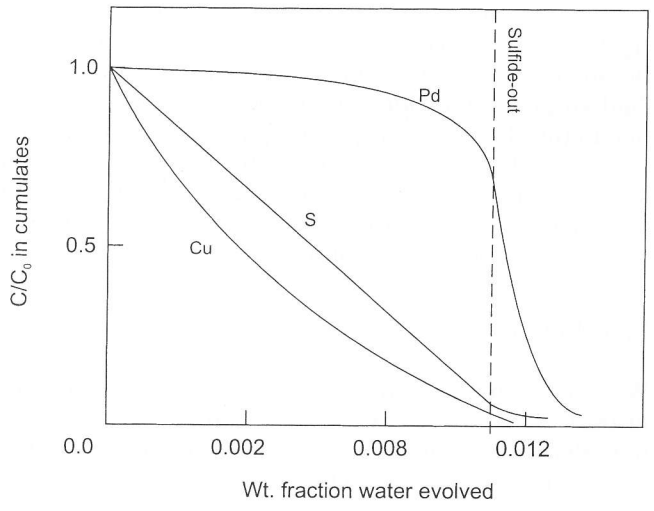

Fig. 3 Effect of degassing and fluid loss on the concentrations of S, Pd and Cu in a crystallizing, partially molten sulfide-bearing assemblage (after Boudreau and McCallum, 1992). Graph of concentration of S, Cu and Pd in residual assemblage (normalized to initial bulk concentration) as a function of wt% fluid evolved during crystallization. Partition coefficients for Cu and Pd between fluid, liquid and sulfide are as discussed in the text. Sulfide-out line is the point at which fluid separation has resorbed all initial sulfide

The rightmost graph of Fig. 4 shows the evolution of the sulfide distribution and the accompanying distribution of metals as the solidification/degassing zones migrate through the growing pile of cumulates. Note that the crystal pile actually develops two reaction fronts. The main reaction front of interest is that resulting from the loss of sulfide by the degassing of interstitial liquids. However, a second occurs higher in the crystal pile at the top of the fluid-saturated zone. Here, an increase in sulfur (as sulfide) occurs as S-bearing fluid redissolves in a liquid already sulfide saturated. The amount of sulfide precipitated is a function of the amount of sulfide carried in the fluid as well as the degree to which the interstitial liquid is undersaturated in fluid. A liquid initially far from fluid saturation will dissolve more fluid and hence precipitate proportionally more sulfide. This additional sulfide is later lost to eventual solidification and degassing.

The Pd loss from the cumulate sequence is trivial until most sulfide is lost, after which the fluid becomes the next best host. The Pd liberated as the last sulfide dissolves is carried upward (a very short distance) until the fluid encounters sulfide-bearing assemblages, at

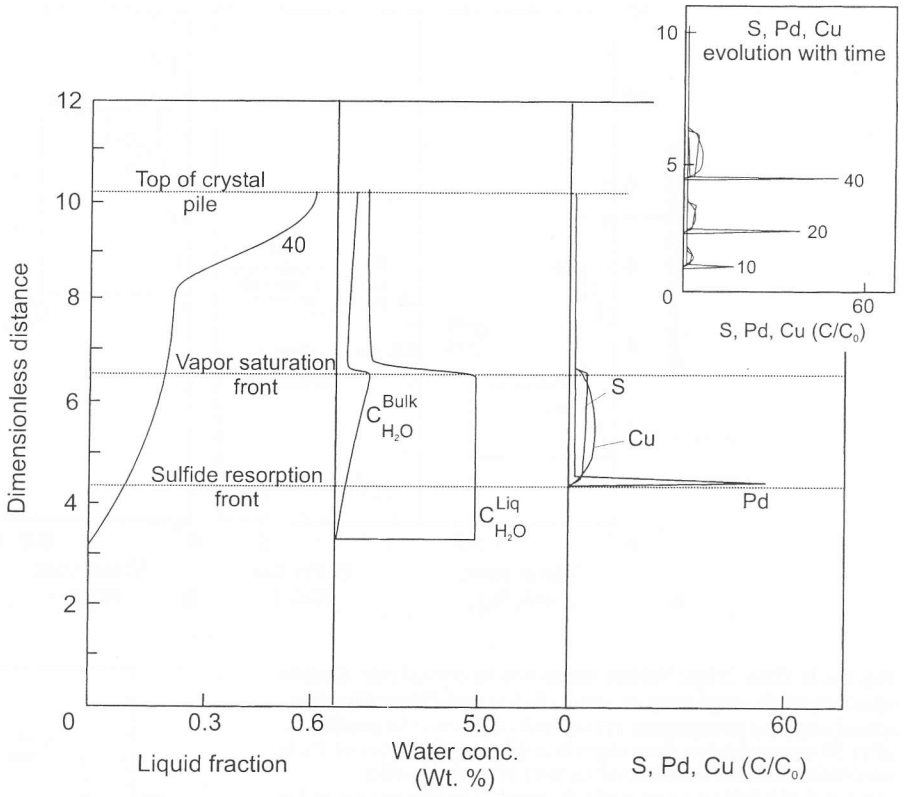

Fig. 4 Case 1: effect of fluid separation and migration during solidification of a compacting crystal pile on the distribution of water, S, Cu and Pd after 40 dimensionless time steps. *Left* plot is fraction of liquid; the top of the crystal pile is at approximately 10 dimensionless units, and the cumulate section between 0 and 3.3 dimensionless units has completely crystallized. The center plot shows the bulk water content, $C^{Bulk}_{H_2O}$ and water concentration of the interstitial liquid, $C^{liq}_{H_2O}$. The region between 3.3 and 6.5 dimensionless units is the fluid-saturated zone. The *right* graph shows the bulk concentrations of S, Cu and Pd relative to their initial concentration. Note the peak in Pd enrichment occurs at the sulfide-dissolution front. *Inset* shows development of ore-element profiles at 10, 20 and 40 dimensionless time steps, respectively

which point the Pd is strongly partitioned into the sulfide. Copper behaves similarly, but is less strongly partitioned into sulfide. Consequently Cu is not as strongly concentrated and is offset to higher stratigraphic levels.

The net effect over time is that both a sulfide-enriched zone and a sulfide dissolution front migrate upward and the Pd is concentrated at the dissolution front. The peak in Cu is above this resorption front, and broadly corresponds to the high sulfur/sulfide zone initially deposited at the fluid-saturation front.

While the size/width of the peaks can be modified by changing, say, the fluid/liquid partition coefficients, the relative position of Pd below the Cu peak will remain as long as Pd has a slower chemical transport velocity than Cu. Thus, a lower Pd sulfide liquid/silicate liquid distribution coefficient (or a higher solubility in the fluid) would lead to a broader Pd peak.

Finally, although we used a simple fluid evolution model, the model does reproduce many of the features observed in PGE-base metal offsets in layered intrusions. Thus Pd is associated with zones of higher than normal (background) sulfide modal amounts, the Pd peak is below that of the main zone of sulfide enrichment, very little Pd occurs in the uppermost part of the sulfide-enriched zone and Cu largely follows bulk sulfur concentrations.

Case 2, degassing of a crystal pile that is not initially sulfide saturated in the lower portions

Figure 5 shows a case similar that of case 1. However, in this instance it is assumed that the initial magma does not become sulfide saturated until after the crystal pile has grown to 5 dimensionless units. Figure 5a shows the system evolution after 30 time steps, at which point the pile is about 6 units thick and has crystallized about 1 unit of sulfide-bearing cumulates at the top of the crystal pile. The top of the fluid-saturation zone is at 4 units but has not yet reached the sulfide-saturation zone. Note, however, that a small peak in S concentration still forms at the top of the fluid-saturation zone as S leached from underlying interstitial liquid is added to the fluid-undersaturated liquid at this level. Although not evident because of the concentration normalization used in the figure, a modest Pd peak is associated with this small peak. Very little Pd concentrates at this lower peak because the interstitial liquid, the only host for Pd in the lower part of the pile, contains much less than is typically concentrated in a cumulus sulfide phase. Consequently, longer migration zones are required to build up high Pd concentrations. However, this case does illustrate that even an initially sulfide undersaturated crystal pile can locally precipitate sulfide-enriched zones that may show small PGE enrichments as fluid migrates upward.

After 60 time steps, the fluid-saturated zone has progressed well into the sulfide-saturated zone and produces the characteristic element peaks as seen previously (Fig. 5b). However, in this case, because there is a large amount of water relative to the amount of sulfur in the system sulfide is moved quite easily. In consequence, the S and Cu peaks are narrower and they develop closer to the top of the fluid-saturation zone.

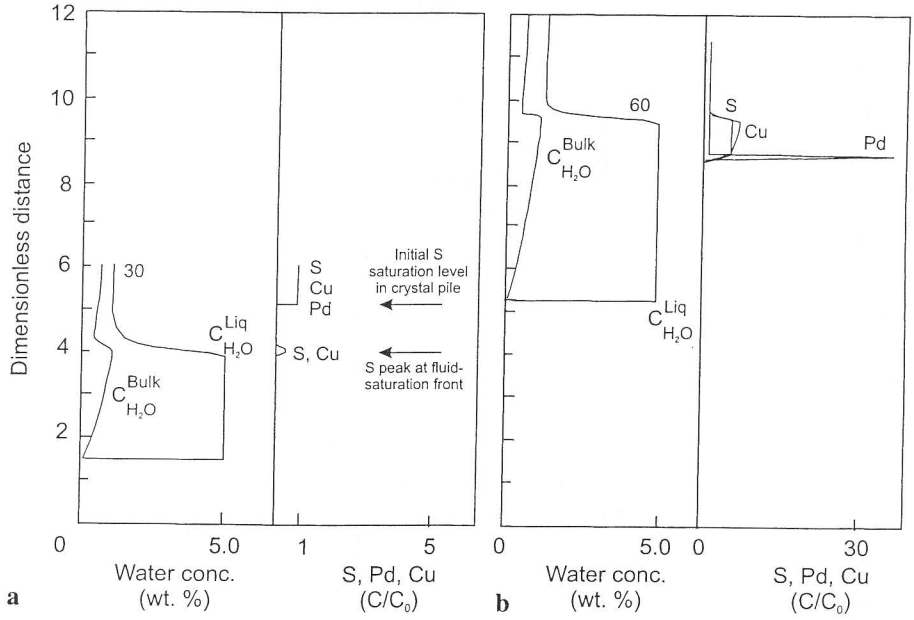

Fig. 5a, b Case 2: late Sulfide saturation in crystal pile. Graphs again show the evolution of water, S, Cu and Pd profiles in a solidifying and compacting crystal pile: **a** shows the profiles after 30 dimensionless time steps; **b** at 60 time steps (ore-element concentrations are normalized to that of initial, sulfide-saturated assemblage; note scale changes). The situation is as for Fig. 4, but in this case the cumulate section is not initially sulfide saturated below 5 dimensionless units. Note in **a** the small sulfide peak that forms at the top of the fluid-saturated zone as sulfur-bearing fluid is added to vapor-undersaturated liquid, inducing sulfide saturation. Note also that all metal concentrations are normalized to initial concentrations typical of the sulfide-saturated cumulates at top of crystal pile

Case 3, slow cooling relative to compaction

Figures 6 and 7 show two other phenomena that may occur when the rate of cooling is slow or fast relative to the rate of compaction. In Fig. 6, the cooling rate at the bottom is only 20% of that in Fig. 4. Once the solidification front advances a short distance into the crystal pile, solidification slows substantially and compaction becomes more important in controlling the amount of interstitial liquid. In this case, all chemical and reaction fronts, but particularly the PGE front, become stalled. This arises because the loss of interstitial liquid by compaction does not allow enough fluid to be evolved to allow the fronts to move faster than the solidification/compaction front at the bottom of the fluid-saturated zone. The eventual result is that the fronts become frozen in the liquid-poor crystal pile.

Case 4, cooling rapid relative to compaction

Figure 7 depicts the opposite case where cooling is relatively rapid compared with compaction. In this case the cooling rate at the bottom is twice as fast as for Fig. 4,

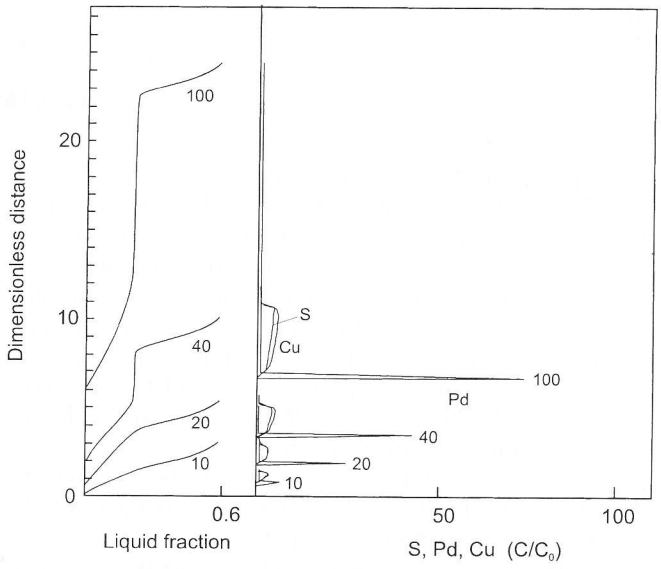

Fig. 6 Case 3: slow cooling case. Similar to that of case 1 shown in Fig. 4, but in this case the cooling rate at the bottom is only 20% of that used in case 1 (1 °C per dimensionless time step). Liquid fraction and S, Cu, and Pd profiles are shown after 10, 20, 40 and 100 dimensionless time steps. Note that at 100 time steps, the Pd chemical front is essentially at the solidification front

and the initial water content of the liquid is 2.0 wt% instead of 1.0 wt%. The rapid evolution of fluid from crystallizing interstitial liquids causes the fluid-saturated zone to reach the upper part of the crystal pile where compaction is relatively rapid. In this instance volatile-saturated interstitial liquids can actually be compacted out of the crystal pile to mix with the liquid in the chamber. The effect of the addition of volatiles to the resident magma in the chamber is that nucleation and growth of the crystal pile should stop. (This is modeled by simply halting the growth of the crystal pile once the

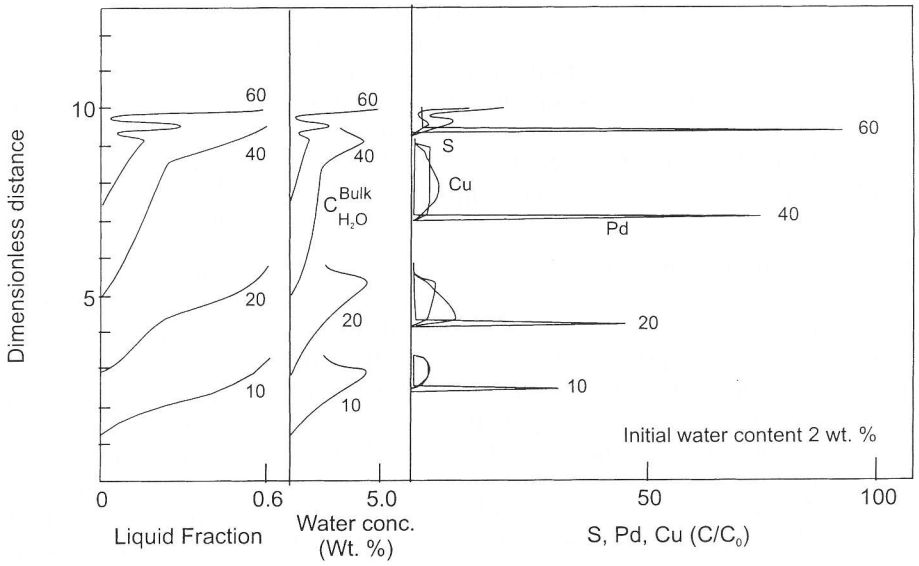

Fig. 7 Case 4: fast cooling, wet magma case. Similar to case 1 shown in Fig. 4, but in this instance the cooling rate at the base is twice as high (10 °C per dimensionless time step) and water content of the initial liquid is twice that for case 1 (2 wt% H_2O). Shown are liquid fractions, bulk water concentrations and S, Cu and Pd element concentrations, the latter normalized to initial starting concentrations. Profiles are shown at 10, 20, 40 and 60 dimensionless time steps

fluid-saturated liquids reach the top of the crystal pile. In addition, the mass of liquid in the chamber above the floor is assumed to be large enough to absorb all fluid evolved from the crystal pile without itself becoming fluid saturated.) Halting the growth of the crystal pile causes the development of porosity waves in the upper part of the pile. In a more realist case, these porosity waves may cause the sulfide-enrichment zone and associated metal fronts to break into several zones as they lead to changes in bulk composition (see Discussion). In addition, the sulfur/metal fronts eventually converge at the now fixed fluid-saturation boundary defined by the top of the crystal pile.

Discussion

The model presented above improves on the simple assumption of the reaction-reaction model presented in the first part of the paper. However, the model is general, illustrative of a process, and is not meant specifically to describe what has occurred in any given intrusion. This is because it also involves a rather simple set of assumptions, including complete equilibration of the system at all times and constant partition coefficients. In addition to these problems, one can envision a number of complications that can occur in a real intrusion, as discussed below.

Nature of the fluid-saturated zone

In the model, the exsolved fluid is assumed to move upward immediately once it separates from the interstitial liquid. In reality, the fluid-saturated zone may consist of a "bubble zone". While the bubbles are small, they may not migrate upward readily through the crystal framework except as aided by compaction. In this case, the fluid/bubbles would initially move upward with the interstitial liquid and would move as a uniform zone through the pile. Over time, however, the bubbles will become large and numerous enough such that they rise more easily. In this case, bubbles moving up from below could combine with smaller bubbles higher in the crystal pile to cause a cascade effect of sudden fluid movement through the crystal pile. If the fluid flow becomes focused into discrete channels it may form metal-rich pipes (e.g., Stumpfl and Rucklidge 1982; Schiffries 1982; Boudreau and McCallum 1986). Alternatively, a focused fluid flow may escape the pile altogether and form potholes in the top of the crystal pile (e.g., Buntin et al. 1985; Boudreau 1992).

Entrapment of sulfide during crystallization

The infiltration-reaction mechanism discussed here differs from most treatments of infiltration in that the fluid is evolved from the rocks (interstitial liquid) it is infiltrating. Solidification of cumulates may effectively isolate some sulfide that becomes either trapped in, or surrounded by, silicate mineral phases. Alternatively, as noted above, fluid migration may become channeled and not equilibrate with the entire assemblage as it passes through the pile. In this case, some sulfide will remain in the depleted cumulates beneath the reaction front and may record the passage of the metal front, the sulfide having a high PGE/S ratios (Fig. 8). It is nonetheless clear that there must be a net loss of PGE and the base metals for ore-element enrichment fronts to develop.

Saturation in a PGE alloy phase

As the PGE front advances, the metal concentrations and PGE/S ratios can become quite high. In a real situation, the PGE may no longer behave as a trace element and, as sulfur is lost, they may begin to precipitate

zones of PGE metal alloys below the main PGE sulfide front. This may explain instances such as are seen in the Bushveld, where the S-poor, PGE-rich UG-2 chromitite occurs below the Merensky Reef where (in normal Reef) the PGE are associated with sulfide. In this interpretation, the UG-2 PGE represents part of the PGE front left behind as relatively insoluble metal alloys.

Effect of compositional variability

A major limitation of the model is that there is no consideration of compositional variability of the matrix. This is particularly troublesome as modal variability is perhaps one of the most characteristic features of layered intrusions. For example, in the Great Dyke the Main sulfide zone is associated with a marked increase in the Fe/Mg ratio of the bulk assemblage that occurs at the top of the Ultramafic zone (e.g., Wilson 1982). We have previously suggested that this enrichment can occur during compaction as interstitial liquid develops porosity waves beneath the density interface at the ultramafic–mafic transition (Meurer and Boudreau 1996). This enrichment in Fe may itself induce sulfide precipitation as fluids exsolved from underlying magnesian cumulates react with the more Fe-rich silicates via reactions of the type:

$$\underset{\text{Fluid}}{H_2S} + \underset{\text{silicate}}{FeO} = \underset{\text{pyrrhotite}}{FeS} + \underset{\text{fluid}}{H_2O}$$

Because of this stratigraphic variability, more than one metal/sulfide zone may develop as the infiltrating fluid attempts to reequilibrate with different bulk compositions.

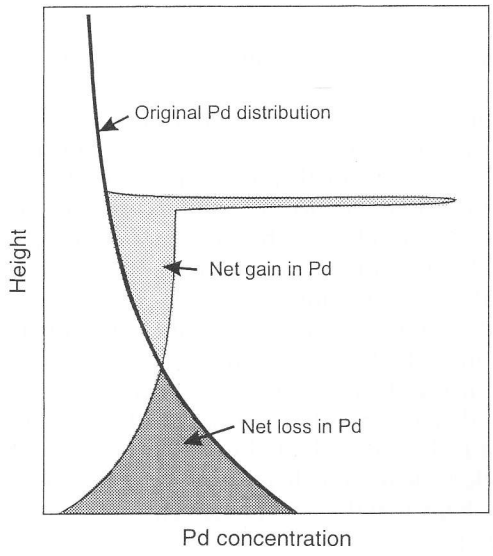

Fig. 8 Example of a more complex Pd distribution profile that may arise in a real intrusion. The original Pd concentration may initially show a simple fractionation trend as shown by the *heavy line*. As the Pd enrichment front migrates through the crystal pile, some of the sulfide in the front may become trapped in the residual assemblage below the front, leading to a new Pd concentration profile as shown by the *light line*. In any case the net gain in Pd (shown by the *light shaded region*) must equal that of the region that experienced a net loss (*dark shaded region*)

Lateral transport of metals

A significant limitation of the model is that it is one dimensional. This may be a reasonable assumption for sills, but many intrusions have a thermal and compositional profile that cannot adequately be described with a one-dimensional model. For example, Andersen et al. (1998) describe the convex-downward layering that characterizes the Pd-Au zones in the Skaergaard as being analogous to a set of "gilt-edged plates" with the gold being preferentially concentrated along the margins of the intrusion. A qualitative explanation for this observation is that fluid migration has a lateral component that moves up-dip toward the margin of the intrusion as well as a vertical component that moves metals up through the intrusion.

Concluding remarks

The model calculations demonstrate several points:

1. The appearance of PGE-enriched sulfide zones in layered intrusions can be explained as the result of migrating sulfide enrichment-resorption fronts accompanying degassing of interstitial liquids and need not be the direct result of sulfide saturation in the magma chamber. In this respect, high PGE/S ratios can be produced by such a chromatographic mechanism without the need to call on high silicate liquid/sulfide liquid mass ratios (R-values; Campbell et al. 1983) of conventional magmatic sulfide-saturation models.
2. The observed ore-element offsets can be produced during the migration of the sulfide resorption front owing to different chemical velocities of the PGE compared to the base metals and gold. The slower transport velocity of Pt and Pd is primarily a consequence of their high affinity for sulfide.
3. The separating fluid need not, in a general sense, "transport" significant PGE except immediately at the sulfide resorption front. Fluid migrating below or above the sulfide resorption front may contain very little of the PGE in solution. Below the front, the PGE have already been lost and thus cannot supply significant PGE to the fluid, whereas above the front the metals are mostly held in the sulfide phase.
4. The degree of PGE enrichment is a function of the length the chromatographic front travels. The longer the front travels, the higher are the resulting PGE concentrations. This explains why high-grade PGE zones typically do not occur along the lower contact of layered intrusions and instead require some thickness of cumulates beneath them.

Acknowledgements This work was improved by the reviews of C. Ballhaus and J. Arnason. This work was supported through NSF grants EAR 94-17144 and EAR 97-05507.

References

Andersen JCØ, Rasmussen H, Nielsen TFD, Ronsbo JG (1998) The triple group and the Platinova gold and palladium reefs in the Skeargaard intrusion: stratigraphic and petrographic relations. Econ Geol 93: 488–509

Ballhaus C, Stumpfl EF (1985) Occurrence and petrological significance of graphite in the Upper Critical zone, western Bushveld complex, South Africa. Earth Planet Sci Let 74: 58–68

Ballhaus C, Stumpfl EF (1986) Sulfide and platinum mineralization in the Merensky reef: evidence from hydrous silicates and fluid inclusions. Contrib Mineral Petrol 94: 193–204

Ballhaus C, Ryan CG, Mernagh TP, Green DH (1994) The partitioning of Fe, Ni, Cu, Pt and Au between sulfide, metal and fluid phases: a pilot study. Geochim Cosmochim Acta 58: 811–826

Barnes SJ (1993) Partitioning of the platinum group elements and gold between silicate and sulphide magmas in the Munni Munni Complex, Western Australia. Geochim Cosmochim Acta 57: 1277–1290

Bird DK, Brooks CK, Gannicott RA, Turner PA (1991) A gold-bearing horizon in the Skaergaard intrusion, East Greenland. Econ Geol 86: 1083–1092

Bird DK, Arnason JG, Brandriss ME, Nevle RJ, Radford G, Bernstein S, Gannicott RA and Kelemen PB (1995) A gold-bearing horizon in the Kap Edvard Holm complex, East Greenland. Econ Geol 90: 1288–1300

Borisov A, Palme H (1997) Experimental determination of the solubility of platinum in silicate melts. Geochim Cosmochim Acta 61: 4349–4357

Borisov A, Palme H, Spettel B (1994) The solubility of Pd in silicate melts: implications for core formation in the Earth. Geochim Cosmochim Acta 58: 705–716

Boudreau AE (1992) Volatile fluid overpressure in layered intrusions and the formation of potholes. Aust J Earth Sci 39: 277–287

Boudreau AE, McCallum IS (1986) Investigations of the Stillwater Complex. III. The Picket Pin Pt/Pd deposit. Econ Geol 81: 1953–1975

Boudreau AE, McCallum IS (1992) Concentration of platinum-group elements by magmatic fluids in layered intrusions. Econ Geol 87: 1830–1848

Boudreau AE, Stewart MA, Spivack AJ (1997) Stable Cl-isotopes and origin of high-Cl magmas of the Stillwater Complex, Montana. Geology 25: 791–794

Buntin TJ, Grandstaff DE, Ulmer GC, Gold DP (1985) A pilot study of geochemical and redox relationships between potholes and adjacent normal Merenesky Reef of the Bushveld complex. Econ Geol 80: 975–987

Campbell IH, Naldrett AJ, Barnes SJ (1983) A model for the origin of the platinum-rich sulphide horizons in the Bushveld and Stillwater complexes. J Petrol 24: 33–165

Fleet ME, Stone WE, Crockett JH (1991) Partitioning of palladium, iridium and platinum between sulfide liquid and basalt melt: effects of melt composition, concentration and oxygen fugacity. Geochim Cosmochim Acta 55: 2545–2554

Godard M, Bodinier J-L, Vasseur G (1995) Effects of mineralogical reactions on trace element redistributions in mantle rocks during percolation processes: a chromatographic approach. Earth Planet Sci Lett 133: 449–461

Hoatson DM, Keays RR (1989) Formation of platiniferous sulfide horizons by crystal fractionation and magma mixing in the Munni Munni layered intrusion, West Pilbara Block, Western Australia. Econ Geol 84: 1775–1804

Hsu LC, Lecher PJ, Nelson JH (1991) Hydrothermal solubility of palladium in chloride solutions from 300 to 700 °C: preliminary experimental results. Econ Geol 86: 422–427

McKenzie D (1984) The generation and compaction of partially molten rock. J Petrol 25: 713–765

Meurer WP, Boudreau AE (1996) Compaction of density-stratified cumulates: effect on trapped liquid distribution. J Geol 104: 115–120

Meurer WP, Willmore C, Boudreau AE (1998) Metal redistribution during fluid exsolution and migration in the Middle Banded Series of the Stillwater complex Montana. Lithos (in press)

Oberthür T, Weiser TW, Müller P, Lodziak J, Cabri LJ (1998) New observations on the distribution of platinum group elements (PGE) and minerals (PGM) in the MSZ at Hartley Mine, Great Dyke, Zimbabwe (abstract). In: 8th Int Pt Symp Abstr, S Afr Inst Min Metall, Johannesburg, pp 293–296

Peach CL, Mathez EA, Keays RR (1990) Sulfide melt-silicate melt distribution coefficients for noble metals and other chalcophile elements as deduced from MORB: implications for partial melting. Geochim Cosmochim Acta 54: 3379–3389

Peach CL, Mathez EA, Keays RR, Reeves SJ (1994) Experimentally determined sulfide melt-silicate melt partition coefficients for iridium and palladium. Chem Geol 117: 361–377

Prendergast MD, Keays RR (1989) Controls on platinum-group element mineralization and the origin of the PGE-rich Main Sulphide Zone in the Wedza Subchamber of the Great Dyke Zimbabwe: implications for the genesis of, and exploration for, stratiform PGE mineralization in layered intrusions. In: Prendergast MD, Jones MJ (eds) Magmatic sulphides – The Zimbabwe volume London Inst Min Metall, London, pp 43–70

Prendergast MD, Wilson AH (1989) The Great Dyke of Zimbabwe. II. Mineralization and mineral deposits. In: Prendergast MD, Jones MJ (eds) Magmatic sulphides – The Zimbabwe volume London Inst Min Metall, Lonon, pp 21–41

Rajamani V, Naldrett AJ (1978) Partitioning of Fe, Co, Ni and Cu between sulfide liquid and basaltic melts and the composition of Ni-Cu sulfide deposits. Econ Geol 73: 82–93

Sassani DC, Shock EL (1990) Speciation of palladium in aqueous magmatic-hydrothermal solutions. Geology 18: 925–928

Schiffries CM (1982) The petrogenesis of a platiniferous dunite pipe in the Bushveld complex: infiltration metasomatism by a chloride solution. Econ Geol 77: 1439–1453

Shi P (1992) Fluid fugacities and phase equilibria in the Fe-Si-O-H-S system. Am Mineral 77: 1050–1066

Shirley DN (1986) Compaction of igneous cumulates. J Geol 94: 795–809

Sobolev AV, Chaussidon M (1996) H_2O concentrations in primary melts from supra-subduction zones and mid-ocean ridges: implications for H_2O storage and recycling in the mantle. Earth Planet Sci Lett 137: 45–55

Stone WE, Crocket JH, Fleet ME (1990) Partitioning of palladium, iridium, platinum, and gold between sulfide liquid and basalt melt at 1200 °C. Geochim Cosmochim Acta 54: 2341–2344

Stumpfl EF, Rucklidge JC (1982) The platiniferous dunite pipes of the eastern Bushveld. Econ Geol 77: 1419–1431

Wilson AH (1982) The geology of the Great 'Dyke', Zimbabwe: the ultramafic rocks. J Petrol 23: 240–292